Influence of infill settings on the flexural properties of 3D printed ABS plus polymer parts in bending loading

Moein Moradi [1], Ramin Hashemi [2]*, Ali Hosseinzadeh [3], Mehdi Kasaeian-Naeini [4]

1, 2, and 4. School of Mechanical Engineering, Iran University of Science and Technology, Tehran 16846-13114, Iran

3. Department of Mechanical Engineering, Ferdowsi University of Mashhad, Mashhad, Iran.

*Corresponding author: Ramin Hashemi (E-mail: rhashemi@iust.ac.ir)

Abstract:

One of the most commonly used techniques in 3D printing is Fused Deposition Modeling (FDM). Despite its widespread adoption, creating functional parts with suitable mechanical properties remains a significant challenge. Previous studies have often focused on various aspects of FDM. Still, there remains a lack of comprehensive research addressing the flexural properties of 3D printed ABS plus polymer parts under bending loads. This gap in the literature motivated the current study. The manufacturing parameters in the FDM process, such as infill density (ID) (20, 50, and 80 percent), layer thickness (LT) (0.1, 0.2, and 0.3 mm), and raster angle (RA) (0, 45, and 90 degrees) were investigated to understand their mutual influence on the bending mechanical properties at ambient temperature through experimental design and analysis of variance. Reinforced ABS polymer filament was utilized in this research. The parameters were studied using the response surface method (RSM) based on the central composite design (CCD), employing quadratic regression equations for all responses to determine the model coefficients. Analysis of variance revealed that the raster angle is the most critical factor influencing the bending response, as it directly affects load transfer to the specimen. The optimal parameters identified for maximum bending strength were ID = 78.277%, LT = 0.295 mm, and RA = 1.599 degrees. the bending strength is maximum in thick layers and low raster angles.

Keywords:

Fused Deposition Modeling, test design, mechanical properties, three-point bending

1. Introduction

Polymer materials and their developments have increased so much in recent decades that it is impossible to imagine the world without polymers. The increase in these applications is due to the reasonable price, suitable mechanical properties, corrosion resistance, low density, and convenient and easy access to all polymers due to the vast country's oil and gas resources. 3D printing is used in various manufacturing sectors such as aerospace, automobiles, bioengineering, aerospace [1], building [2], and jewelry [3]. The additive manufacturing process has advantages such as producing parts with complex shapes with shorter production times and reducing costs compared to traditional manufacturing methods [4].

Various techniques exist for the additive manufacturing (AM) of metal, ceramic, polymer, and composite components. The Fused Filament Fabrication (FFF) is the most common method for making polymer pieces [5]. In this approach, polymers of thermoplastic in the form of threads (known as filaments) are fed into a liquefier using gears. The filament is then heated to a specific temperature based on its type until it reaches a molten state with the appropriate viscosity. The extruder moves along the X and Y axes to create a layer, and successive layers are formed by the extruder's movement and the filament's withdrawal in the Z direction. Thus, the final piece is made layer by layer. However, the mechanical properties and surface quality of parts produced via FFF are generally considered inferior to those manufactured using traditional methods such as injection molding, extrusion, and compression molding [6]. The mechanical properties and print quality of FFF parts are influenced by various process parameters, including raster angle, shell number, air gap, printing speed, raster width, layer thickness, infill density, and orientation of build [7]. By optimizing these parameters, the limitations in mechanical properties and fabrication quality can be mitigated to some extent.

Garg and Bhattacharya [8] investigated the fracture demeanor of ABS pieces with varying layer thicknesses and raster angles using experimental and numerical methods. The researchers utilized the finite element method to simulate the inter- and intra-layer bonds in the adhesive. Their analysis revealed that as the layer thickness increases, the elongation also increases. In addition, they observed that the ultimate tensile strength (UTS) initially decreases and then subsequently increases. Fractions occur for zero and 90-degree raster angles due to raster breakage and delamination, respectively. In their study, Dawoud et al. [9] compared the mechanical properties of ABS parts manufactured using injection molding and Fused Deposition Modeling (FDM). They discovered that the injection-molded specimens displayed superior mechanical properties. However, they achieved comparable mechanical properties in FDM by employing a negative air gap and a raster angle of ±45 degrees.

Nomani et al. [10] investigated the tensile properties and compressive strength of ABS parts with varying layer thicknesses. They observed that a decreased layer thickness improved mechanical properties due to more uniform deposition layers and fewer gaps. In contrast, an increased layer thickness reduced the production time of the specimens. Rodriguez-Panes et al. [11] extensively studied the tensile properties of two commonly used filaments in FFF: ABS and PLA. They investigated the effects of variable parameters such as layer thickness, infill density, and orientation of the build. Among these, infill density was the most significant factor for both filament types. For ABS specimens, layer thickness had minimal impact on tensile properties, whereas mechanical properties diminished with increasing layer thickness for PLA.

Additionally, they observed that In the ideal parameter combination for ABS, the tensile properties were still 22% lower than the raw filament material. Kannan and Ramamoorthy [12] examined the mechanical properties of specimens made from PC, ABS, and PC-ABS, which are frequently used in the aerospace industry. They found that PC-ABS's ultimate tensile strength (UTS) was 24% higher than that of pure ABS and 16% higher than that of pure PC. Furthermore, the elastic modulus of PC-ABS was 24% higher than that of ABS and 41% higher than PC's.

Khalili and et al. [13] examined how layer height, print speed, and nozzle temperature influence the tensile and flexural properties of polylactic acid/continuous carbon fiber (PLA/CCF) composites. An

and other authors [14] researched laser polishing as a post-processing technique to reduce surface roughness in ABS and Nylon parts produced via Fused Deposition Modeling (FDM). Rendas and other authors [15] have researched the effects of various printing parameters—such as nozzle temperature, zone heater temperature, layer height, and extruder multiplier—on the interfacial adhesion and subsequent mechanical performance of PEEK (Polyether ether ketone) 3D prints. They performed Design of Experiment (DoE) studies, utilizing the Taguchi method and ANOVA analysis to determine the optimal parameter combinations and their respective contributions to the overall performance. Their findings provide valuable insights into the intricate relationships between these printing parameters and the resulting mechanical characteristics of PEEK prints. Zou and other authors [16] explored the fracture toughness and flexural strengths of CTB through 3-point bending tests and scanning electron microscopy (SEM) observations. Their lab testing results demonstrated that the application of 3D-PP significantly enhanced the flexural and deflection properties of CTB. The bending strength of the CTB structures fabricated with 3D-printed polymers was found to be 1.72 MPa, indicating a substantial increase of 409% compared to the control specimens (N-3D-PP). Esfe and his colleagues [17] conducted a study predicting the dynamic viscosity of a SiO2 (60%)-MWCNT (40%) hybrid nanofluid in SAE40 oil, using various response surface models (RSM) and identifying the Quartic model as the most effective based on quality indicators. Esfe et al. [18] conducted research evaluating and comparing two novel hybrid nanofluids (HNF) using experimental and statistical methods, specifically response surface methodology (RSM), to identify one suitable for industrial application. Esfe et al. [19] investigated the rheological properties of MWCNT nanofluids based on thermal oil, finding that increasing solid volume fraction enhances thermal conductivity, viscosity, and density while reducing thermal expansion. Their study employed response surface methodology (RSM) and multilayer perceptron (MLP) modeling, achieving high accuracy in predicting these properties.

Testing always involves cost and time. Therefore, conducting practical tests that provide the most information with the least cost and time will be very useful. Many factors and parameters may affect the mechanical properties of polymer parts made by FDM. One of the essential goals of experiment design is to identify the parameters that have the most significant effect on the output. By identifying these parameters and removing parameters that do not affect the output, the number of tests can be significantly reduced, reducing costs.

ABS Plus filament was selected for this study due to its well-documented properties, including durability, impact resistance, and ease of processing. It is a popular choice in various applications, such as 3D printing. The specific manufacturing process utilized, combined with ABS Plus, enables an exploration of the material's performance under different conditions, providing insights into how processing parameters can influence its mechanical properties. Bending was identified as an essential property for focus because it is critical for evaluating the material's structural integrity in real-world applications. Understanding bending behavior is crucial in determining suitability for various applications where load-bearing capability is essential.

In this research, the mechanical properties of thermoplastic polymer acrylonitrile butadiene styrene ABS, created by an FDM 3D printer layer by layer, are studied. Standard specimens with different manufacturing conditions are created according to the experimental design and RSM. The investigated mechanical properties include bending properties at ambient temperature. The three-

point bending test and the geometry of the rectangular specimen are used to check the bending properties.

2. Methodology

2.1.Material and method

In this research, Design-Expert software (Stat-Ease, USA). The research utilized the response surface method (RSM) based on the central composite design (CCD), with three repetitions for central points and calculating disproportion. The RSM method can be a suitable option for experiment design because it detects the optimal response values and the influence between them with the least number of experiments. This study investigates the impact of independent variables: infill density (A, ranging from 20 to 80%), layer thickness (B, ranging from 0.1 to 0.3 mm), and raster angle (C, ranging from 0 to 90 degrees) on bending behaviors. The parameter values and their levels are presented in Table 1. The coded levels -1, 0, and +1 represent low, medium, and high, respectively.

Table1. Independent parameter values and design of experiment levels.

			Parameter level		
S.No.	Parameter	Name	-1	0	+1
1.	A	Infill density (%)	20	50	80
2.	B	Layer thickness (mm)	0.1	0.2	0.3
3.	C	Raster angle (degree)	0	45	90

The study utilizes ABS plus polymer filament, 1.75 mm in diameter, known for its enhanced strength and reduced elongation compared to ABS filament [20]. The specimens were prepared according to ASTM D790 [21] Standard, with the dimensions shown in Figure 1. The geometry model was initially created using Catia software before being converted to STL format. Subsequently, this format was fed into the slicer software, facilitating the production of the specimen layer by layer. The 3D printer employed in this study (Creality Ender-6, Shenzhen, China) boasts dimensions of 250 mm × 250 mm × 400 mm. The consistent build parameters can be found in Table 2.

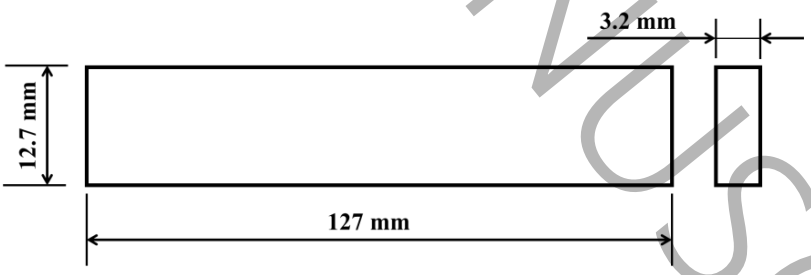

Fig. 1. ASTM D790 standard specifies the dimensions of the bending test specimen.

Table 2. Constant build specs and details

Fixed printing conditions	Description
Base material	ABS plus
Nozzle diameter	0.4 mm
Print speed	60 mm/s
Nozzle temperature	220 ℃
Bed temperature	90 ℃
Print orientation	Flat on bed
Filling pattern	Linear
Extrusion width	0.48 mm
Filament diameter	1.75 mm
Number of shells	2
Number of top and bottom solid layers	2

In prior research, layer thickness, raster angle, and infill density parameters were recognized as factors influencing bending characteristics [11, 22]. Therefore, these three parameters are considered as variable parameters. Three values of 0, 45, and 90 degrees were considered for the raster angle. (Figure 2-a).The layer thickness parameter can be changed according to the nozzle diameter. According to the nozzle diameter of 0.4 mm, the values of 0.1, 0.2, and 0.3 mm have been determined for the thickness of the layer.(Figure 2-b).The infill density parameter has also been selected as the third variable parameter. This parameter is also directly related to the construction time. The lower the infill density or injection percentage, the fewer materials are used, which saves costs and reduces the weight of the final specimen. In this research, infill densities of 20, 50, and 80 (the number of grooves per one centimeter is 4, 10, and 16, respectively for 20, 50 and 80% of infill densities) were used to study the effect of this parameter on mechanical properties. This parameter is shown in Figure 2-c.

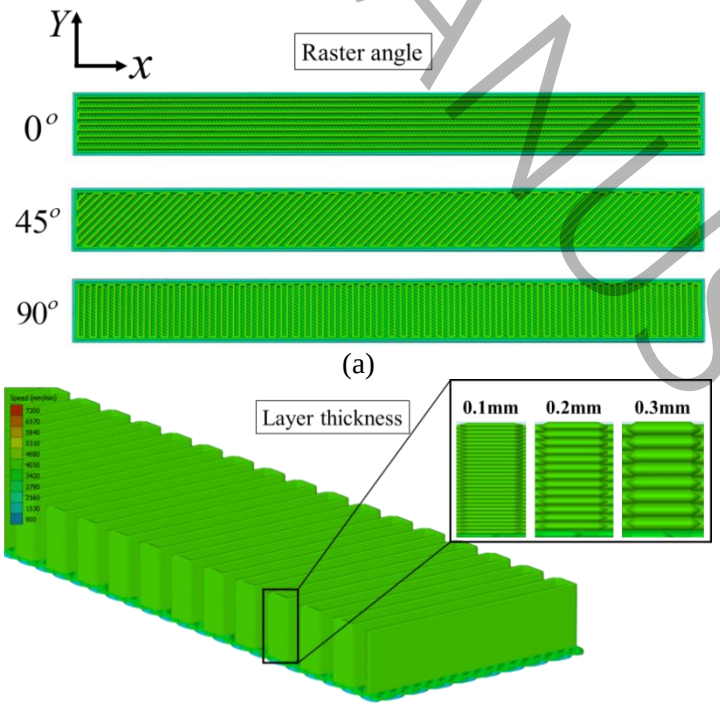

(a)

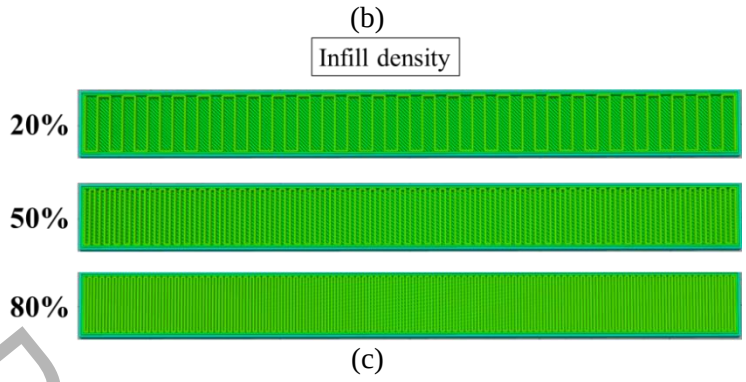

Fig. 2. Schematic depiction of the three variable parameters in fused filament fabrication: (a) raster angle, (b) layer thickness, and (c) infill density.

It should be noted that after preparing the samples by 3D printer, they were separated from the mold and no surface treatment or heat treatment was performed on them.

2.2.Experimental set-up

The geometry of the bending test specimens was designed according to the ASTM D790 standard. The geometry and dimensions of the specimen are first designed in the Catia software, and then the format of the designed specimens is selected to enter the 3D printing machine in STL format. In this research, simplify3D software, which is powerful in the field of rapid prototyping, has been used as a slicer software.

Bending properties may change according to specimen depth, temperature, environmental conditions, and strain rate. As mentioned earlier, the ASTM D790-03 standard was used as a standard test method for the bending properties of plastics and polymers. According to this standard, the printed specimens were kept at a temperature of 23±2°C for at least 40 hours before testing.

Bending tests were conducted using a SANTAM STM-150 machine, which Santam Co. manufactures in Iran. The ratio of the opening of the support to the depth of the specimen should be 16:1, which is the same as seen in Figure 3; considering the depth of 2.3 mm of the specimens made, the distance between the opening of the supports is considered equal to 51 mm. The test continues until the outer surface of the specimen breaks or the maximum strain reaches 5%. The supports and rollers are cylindrical and 8 mm in diameter. The movement rate of the crosshead and grips is calculated according to Equation 1 [21].

$$R = \frac{ZL^2}{6d} \tag{1}$$

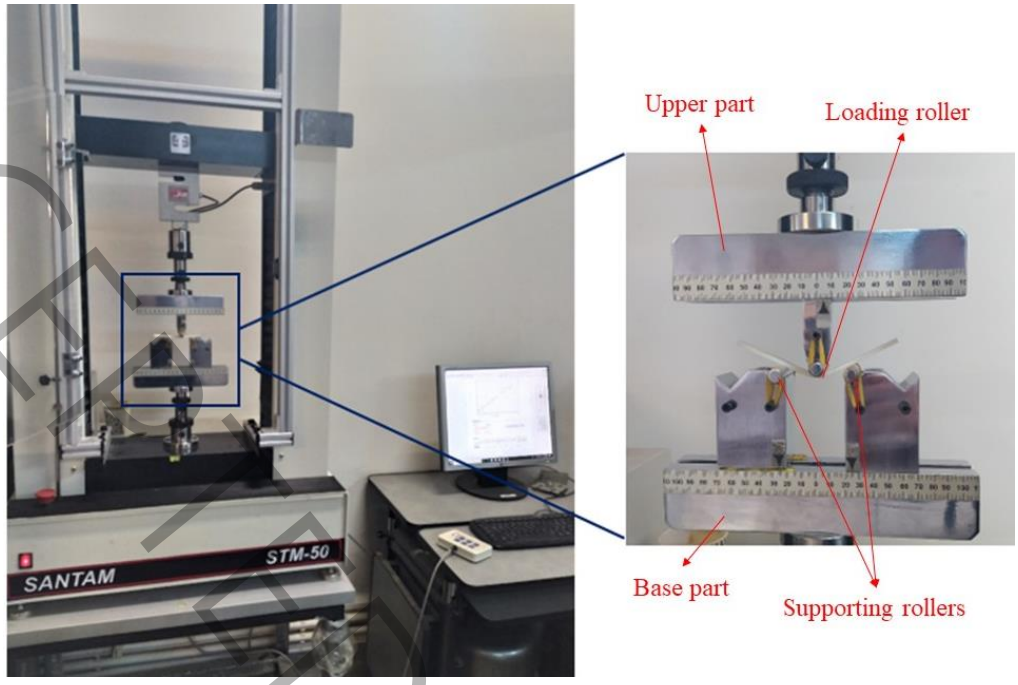

Fig 3. Three-point bending test machine

where R is the movement rate of the grips in mm/min, and Z is the strain rate of the external surface in mm/(mm⁄min), which is considered equal to 0.01. L is the distance of the support in mmm, and d is the depth or thickness of the specimen in mm. According to the value of 0.01 for the strain rate, 51 mm for the support distance, and 2.3 mm for the thickness of the specimen, the value of the movement rate of the grips is equal to 1.4 mm/min. The force-displacement data is saved simultaneously in the Santam device system. The deviation value of the middle of the test specimen is calculated according to Equation 2 [21].

$$D = \frac{rL^2}{6d} \tag{2}$$

D is the deviation value of the middle of the test specimen in mm, and r is the strain value, which is considered equal to 0.05. L is the distance between the supports, and d is the thickness of the specimen. With the placement of L equal to 51 mm and d equal to 3.2 mm, the value of the maximum deviation D equals 6.83 mm. When the deflection of the specimen reaches this value or if failure occurs before that, the test is stopped. When the specimen is placed on the supports and loaded by the roller in the middle, the maximum stress occurs at the midpoint just below the loading roller.

3. Result and discussion

3.1. Stress-strain relationship

ABS polymer is generally an amorphous thermoplastic with numerous molecular chain entanglements in its structure [23]. When stress levels on the specimen exceed a certain threshold, these entanglements start

to unravel, ultimately leading to the failure of the specimen as stress escalates. As per Table 3, 17 specimens are manufactured under varying conditions outlined in the DOE, each being replicated thrice to minimize errors and maintain data consistency. The bending test aims to obtain the optimal parameters of the raster angle, infill density, and layer thickness strings for maximum bending strength. The responses were analyzed using the average of three specimens for each manufacturing condition.

Table 3. Experimental result and design matrix

	Processing Parameters			Response	
Specimen	Infill density (%)	Layer thickness (mm)	Raster angle (°)	Average bending strength (MPa)	Average fracture strain [13] (%)
1	20	0.1	0	28.27	2.822
2	80	0.1	0	52.57	3.158
3	20	0.3	0	38.23	2.04
4	80	0.3	0	54.18	2.886
5	20	0.1	90	9.8	1.299
6	80	0.1	90	15.7	1.596
7	20	0.3	90	27.06	1.45
8	80	0.3	90	32.17	1.624
9	20	0.2	45	20.21	2.529
10	80	0.2	45	32.62	2.888
11	50	0.1	45	18.15	2.331
12	50	0.3	45	32.24	2.132
13	50	0.2	0	40.6	3.559
14	50	0.2	90	15.08	2.419
15	50	0.2	45	24.54	2.961
16	50	0.2	45	23.07	2.94
17	50	0.2	45	21.89	2.78

The test continues until the external surface of the specimen fails or the maximum bending strain reaches 0.05. The bending strength values for each specimen can be seen in Figure 4. The highest and lowest value for bending strength is 54.18 MPa for the fourth specimen and 9.8 MPa for the fifth specimen, and the average value is 28.61 MPa. The bending stress-strain diagram according to the specimens' raster angle can be seen in Figure 5. In none of the specimens with a raster angle of 0 degrees, failure does not occur before the strain limit of 5%. Therefore, the highest strain values are related to the specimens with zero-degree raster angles. Also, in all the specimens with a 90-degree raster angle, except for specimen 7, failure occurs before reaching the 5% strain limit, and for specimens with a 45-degree raster angle, both before and after the 5% strain limit.

As can be seen, early failure of the specimen does not mean low bending strength. For example, specimen eight experiences yielding and failure earlier than specimen 11 but has higher bending strength. The highest modulus and bending strength values are related to the second and fourth specimens. Together with the first specimens, these specimens have the highest bending strain. What these three examples have in common is the zero-degree raster orientation. As can be seen from Figure 6, the specimens show three different types of bending behavior. Some specimens, such as specimen 14, fail before reaching the

5% ultimate strain. The behavior of these specimens is such that the amount of stress does not increase in a region of the diagram with the increase of bending strain. This specimen has reached a yield point. Also, some specimens, such as specimen 8, fail before the specimen reaches the yield stage and 5% limit strain. In this case, the bending strength equals the stress at the fracture point. The behavior of some specimens is similar to that of the first specimen in that failure and yielding do not occur before reaching the limit strain of 5%.

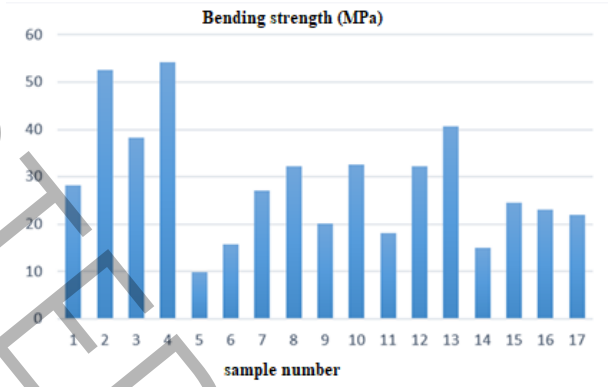

Fig. 4 Average bending strength values for standard specimens in bending test

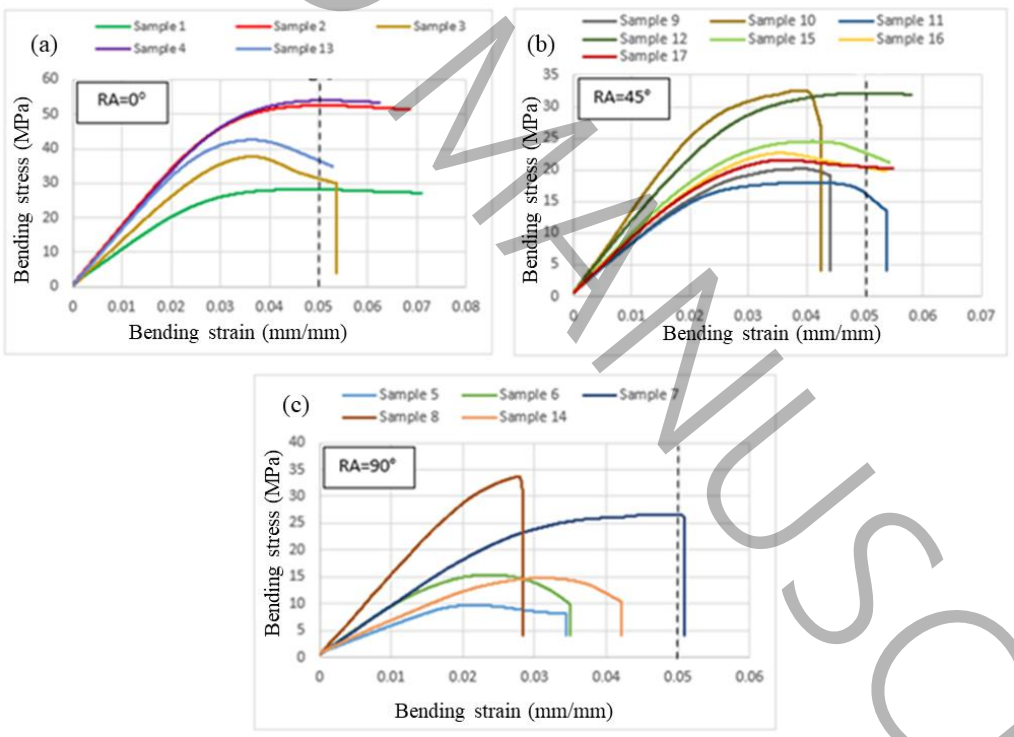

Fig. 5 Bending stress-strain diagram for specimens with raster angle (a) zero degree. (b) 45 °. (c) 90°

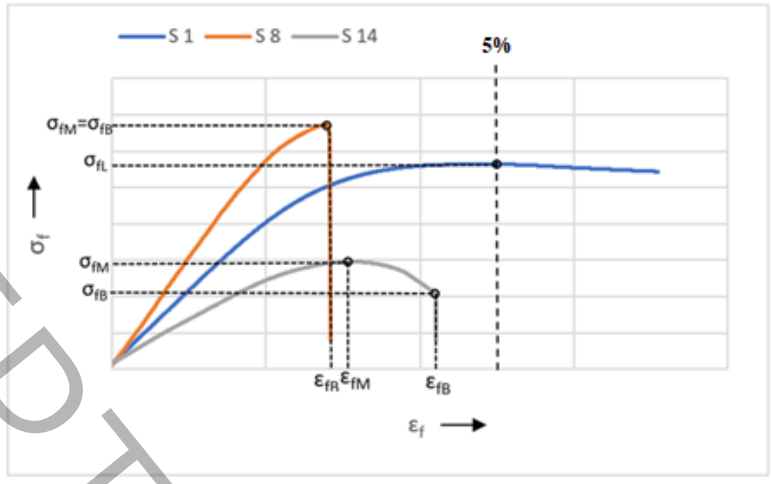

Fig. 6 Different bending test behaviors for specimens with different manufacturing conditions

3.2. Analysis of variance and regression model

Analyzing experimental test results for each response establishes coefficients in the quadratic equation. The quadratic model needs to undergo analysis of variance (ANOVA) to assess the significance of each parameter, their interactions, and the overall model validity for the response. Additionally, various conditions must be met to determine the validity and importance of the models and terms. The P-value and F-value indicate the significance of each term. A P-value below 0.05 indicates the significance of the model or specific term; otherwise, it does not. The results obtained from the bending test can be seen in Table 4. According to the results, the highest bending strength value is related to the fourth specimen with a value of 54.18 MPa and the parameters of the infill density of 80%, the layer thickness is 0.3 millimeters, and the raster angle is 0 degrees. Also, the lowest bending strength value is related to the fifth specimen, with a value of 9.8 MPa and infill density parameters of 20%, layer thickness of 0.1 millimeters, and raster angle of 90 degrees. As indicated in this study, response surface methodology (RSM) utilizing central composite design (CCD) was employed to validate and predict outcomes. This approach enables the attainment of optimal parameter levels and evaluation of individual and interaction effects with fewer experiments.

Consequently, 17 testing conditions, encompassing three replications at the central point, were assessed, considering the various parameters and their levels. In this research, RSM and CCD will be used for design. Also, according to the answers obtained from the experimental tests and the answers predicted by the software, the quadratic model is suggested for the desired design. The analysis of variance for the quadratic model will be shown in Table 4. The quadratic equation is analyzed by means of variance analysis.

Table 4. ANOVA for response surface quadratic model for bending strength

Source	Sum of squares	F value	P value	importance
Model	2465.95	102.87	< 0.0001	significant
A	405.39	152.19	< 0.0001	significant
B	352.72	132.42	< 0.0001	significant
C	1300.51	488.25	< 0.0001	significant
AB	10.44	3.92	0.0882	Not significant
AC	106.68	40.12	0.0004	significant
BC	61.38	23.04	0.0020	significant
A^2	22.62	8.49	0.0225	significant
B^2	7.61	2.86	0.1348	Not significant
C^2	50.25	18.86	0.0034	significant
Lack of Fit	15.12	1.72	0.4078	Not significant

The effect of the obtained data on the bending strength response is shown using F-value and P-value. Data with high F-value and low P-value have the most significant impact on the answer. In the bending test, data with P-values less than 0.05 affect the response, and data with P-values greater than 0.05 are removed from the regression equation due to their non-significant impact on the response. Therefore, the design model and parameters A, B, and C will be significant with P-values less than 0.0001. Also, the mutual influence of A and C parameters and B and C parameters with P-values equal to 0.0004 and 0.002, respectively, on the response is significant and will be present in the regression equation. Also, A^2 and C^2 parameters with P-values of 0.0225 and 0.0034 will impact the answer, respectively. However, AB and B^2 parameters with P-values greater than 0.05 will be removed from the regression equation due to their insignificant effect on the response. Therefore, the coded and true regression equations for bending strength, according to equation (4), are shown in equations 3 and 4, respectively.

$$\text{Flexural strength} = 23.68 + 6.37X_1 + 5.94X_2 - 11.4X_3 - 3.66X_1X_3 + 2.77X_2X_3 + 3.48X_1^2 + 4.90X_3^2 \quad (3)$$

$$\begin{aligned}\text{Flexural strength} &= 26.60742 - 0.052380\ \text{infill density} + 31.69000\ \text{layer thickness} - 0.459575\ \text{raster angle} \\ &-0.002707\ (\text{infill density} \times \text{raster angle}) + 0.615556\ (\text{layer thickness} \times \text{raster angle}) \\ &+0.003864\ (\text{infill density})^2 + 0.002421\ (\text{raster angle})^2\end{aligned} \quad (4)$$

The influence values of each parameter on bending strength can be seen in Figure 7. Based on this data, the raster angle parameter significantly impacts the response. This parameter determines the anisotropy properties of specimens made in different directions. After this parameter, infill density and layer thickness have the most significant effect on bending properties. The infill density parameter is directly related to the amount of material used to make the piece, its weight, and manufacturing cost. Also, as seen in the figure. The mutual influence of density and layer thickness parameters and the second power of layer thickness have a negligible effect on the response.

The raster angle refers to the orientation of the deposition raster in relation to the X-axis of the printer's build platform. Typically, parts printed at a 0° raster angle exhibit the highest strength, whereas those printed at a 90° raster angle tend to show the lowest mechanical performance. This difference in performance is due to the fact that, at 0° orientation, the rasters are aligned with their longitudinal axes during loading, which can lead to failure along these axes. In contrast, when bending loads are applied along the longitudinal axis of the raster, weak intra-raster bonding may cause delamination [24].

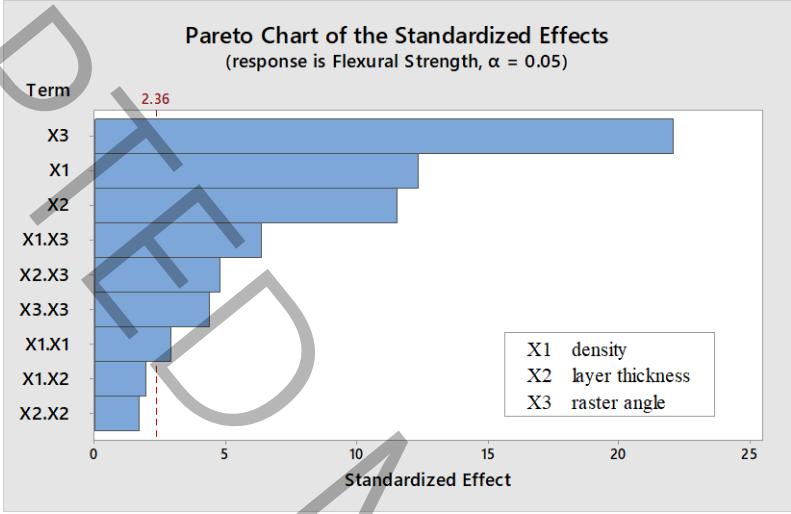

Fig. 7. The relative impact of interaction, individual, and squared terms on bending strength responses

Also, according to Figure 8, it is possible to check the degree of agreement between the data obtained from the experimental tests and the predicted values of the software using the quadratic regression model. This degree of agreement is calculated using the overlap value (R^2). The value of R^2 for flexural strength is equal to 0.9852, which means that 1.1% of the experimental and predicted data do not match. When a specimen is subjected to bending loading, one side experiences compression, and the other experiences tension. The tensile strength of thermoplastic materials is lower than their compressive strength. Thus, the specimen typically fails on the tensile side initially. Consequently, tensile properties play a crucial role in determining bending characteristics.

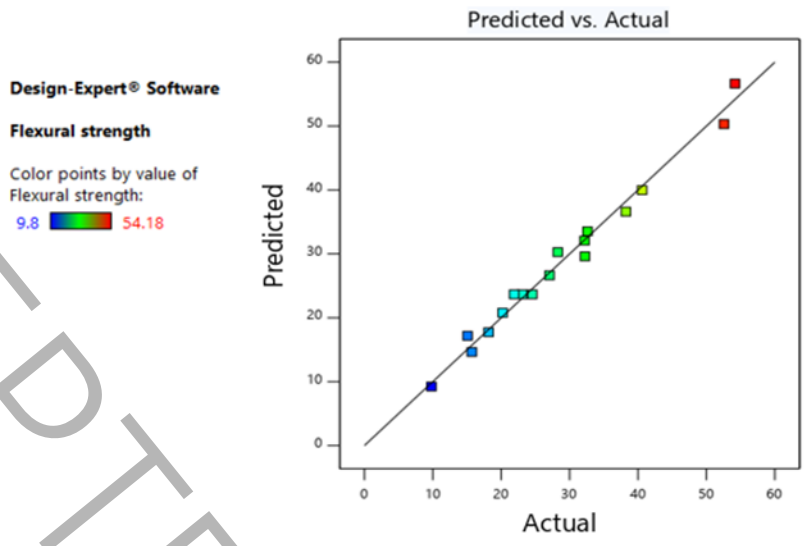

Fig. 8. R^2 correlation coefficient graph related to the bending test

3.3. Effect of parameters on bending characteristics

Figure 9 illustrates the effect of parameters on bending strength. Increasing the density from 20% to 50% does not significantly affect the response. However, with an increase from 50 to 80%, the bending strength shows a visible increase. In fact, with the increase of the density value, the number of holes that are the place of stress concentration and the initiation of cracking and fracture is reduced; hence, the resistance of the specimen against fracture increases. Strings with low thickness cause narrowing and failure to happen sooner.

In contrast, the layer thickness increases, the number of layers is less, and the overlapping area is more, increasing the bending strength. Also, the layer thickness is higher, the cooling rate is lower, the heat capacity is higher, and the higher temperature of the sedimentary filaments is necessary for the fusion between the layers. In the bending test, the raster angle is the response's most critical and practical parameter.

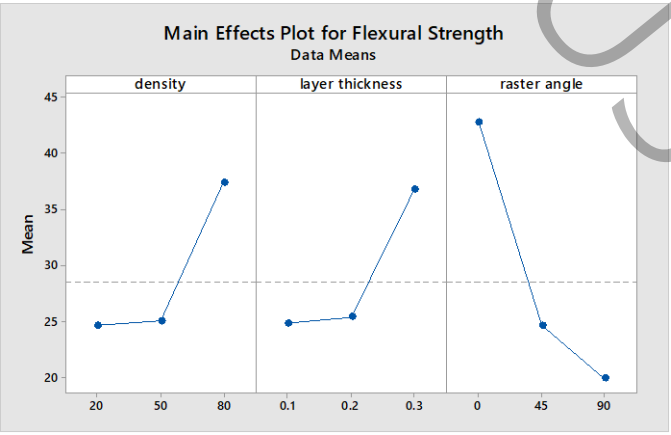

Fig. 9. Impact of production factors on bending strength

As can be seen, the bending strength decreases with the increase of the raster angle. Low raster angles make the strands bear the applied load, but at high raster angles, the strands play a weak role in bearing the load, and the weak inter-layer bonds bear the applied load. Also, layer thickness and density are significantly reduced at high construction angles because the construction layers have a negligible effect on the bending strength at 90-degree raster angles.

Figure 10 shows the mutual influence of the raster angle and density parameters. The highest bending strength values are observed in the red areas of the diagram, which have high infill density and low raster angles. Increasing the raster angle shows a significant drop in bending properties. Figure 11 shows the interaction of the layer thickness parameters and the raster angle at a density of 50%. According to the figure, the bending strength is maximum in thick layers and low raster angles. The optimal construction parameters for the maximum bending strength value include a density of 78.277%, layer thickness of 0.295%, and raster angle of 1.599 degrees. These parameters lead to a bending strength of 54.765 MPa.

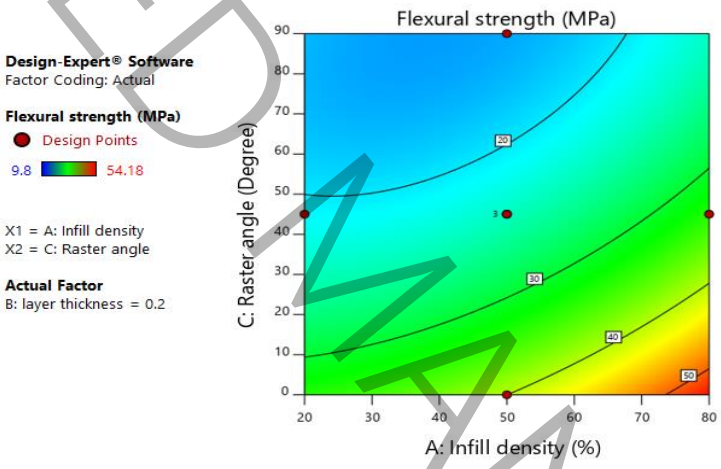

Fig. 10. Mutual Effect of raster angle and density parameters on bending strength in a layer thickness of 0.2 mm

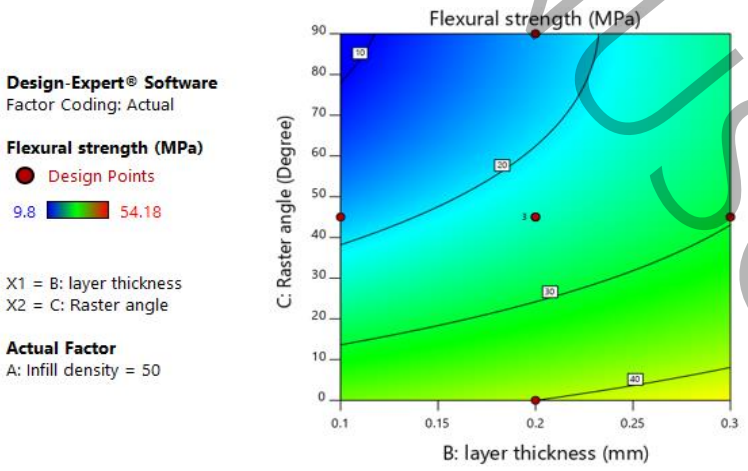

Fig. 11. The mutual Effect of raster angle parameters and layer thickness on bending strength at 50% density

3.4. Failure behavior in bending test

According to Figure 12, three types of failure behavior can occur after loading on the specimens: interlayer failure, intra-layer failure, and a combination of interlayer and intra-layer failure. In specimens with a 90° raster angle, all inter-laminar failure occurs due to weak bonds between layers. In specimens made at 90 degrees, the parameters of layer thickness and density have relatively little effect on the bending strength of the specimen. Because the construction filament has a small load, the interlayer bonds bear most of the load. Due to the weakness of these links, premature failure occurs in the specimen.

For this reason, the lowest amount of bending strain among the specimens is related to the specimens with a raster angle of 90 degrees. In specimens with a 45-degree raster angle, the primary fracture is between layers, while sometimes, intra-layer failure also occurs in this type of specimen. The increase in resistance with better fusion between layers causes intra-layer failure to occur earlier than inter-layer failure. In making specimens with a zero-degree angle, the resistance to bending failure increases dramatically. This increase is because the main construction strands the bending load, and the adhesion between the layers does not play a prominent role in the bending strength. The specimen is bent until the construction strands of the load. Therefore, in this case, intra-layer fracture dominates over inter-layer fracture. The big challenge of the specimens made by FDM is the anisotropic properties of the specimens in different directions. The fabricated specimens have inferior interlayer properties. In fact, due to insufficient fusion between adjacent layers in the specimens, most of the failures are interlayer. Proper bonding between layers is an essential factor for improving mechanical properties. Among the factors that can affect the bonding between layers, we can mention the nozzle's temperature, the melt's viscosity, the cooling rate, and the heat capacity of the sedimentary filaments. Hence, by controlling these factors and optimizing the parameters, we can achieve good bending properties.

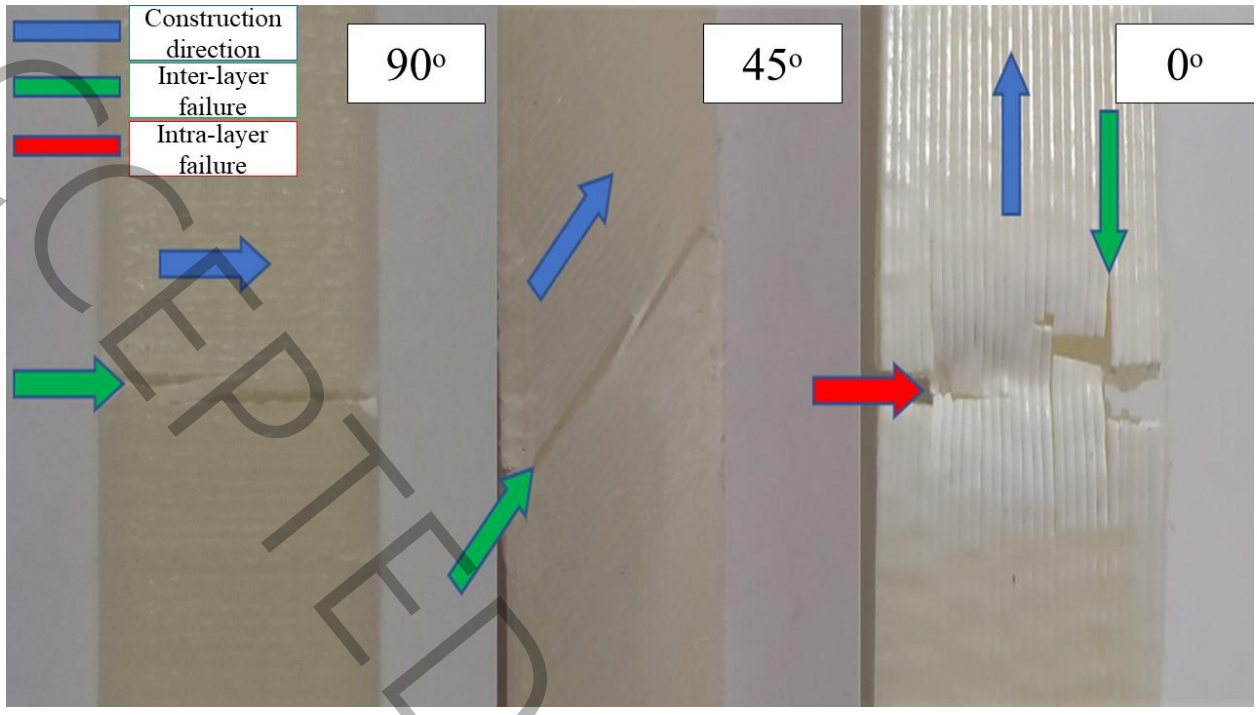

Fig. 12. Intra- and inter-layer failures in bending test

The result show the raster angle refers to the orientation of the printed lines in relation to a reference axis. Results indicate that a raster angle of 0 degrees yields the maximum bending strength, while 90 degrees results in significantly lower strength. At a raster angle of 0 degrees, the filaments are aligned along the direction of the applied load during bending. This alignment maximizes load transfer efficiency, allowing structures to resist bending forces more effectively. Conversely, a 90-degree raster angle represents a perpendicular orientation to the loading direction, which may create weak points where the material cannot support the load effectively. This causes the filaments to fail more easily under stress.

The second factor, layer thickness, influences bonding between layers. Thicker layers can lead to stronger inter-layer adhesion due to the larger surface area for bonding, but can also introduce flaws and inconsistencies. Thicker layers may offer higher strength when the bonding quality is maintained, as sufficient heat can be transferred between layers. However, if the bonding is compromised due to high layer thickness, the structural integrity of the specimen diminishes, possibly leading to a reduction in strength. For optimum performance, the design must achieve a balance where the layer thickness is sufficient to allow for good adhesion without compromising the mechanical integrity of the build.

The infill density affects the internal structure of the printed specimen. Higher infill densities correspond to improved bending strength compared to lower densities. Increasing the infill density reduces the number of voids, therefore decreasing points of stress concentration where failure can initiate. The density in holes and gaps becomes a critical factor in determining strength; fewer voids lead to a more robust internal support structure that can better withstand mechanical loads. It is crucial to note that while increasing infill density enhances strength, this also entails higher material usage and longer build times. Therefore, an optimal balance must be struck between achieving desired mechanical properties and managing production efficiency and costs.

In finally the application of a quadratic model suggests that there are interaction effects between the parameters. For instance, the optimal raster angle might significantly change the influence of infill density on strength, indicating that these parameters do not act independently. Response surface methodology provides a systematic approach to exploring the relationship between multiple factors and responses. In this instance, it reveals how various combinations of raster angle, layer thickness, and infill density can be optimized to achieve desirable mechanical properties without conducting exhaustive testing. The identification of an optimal set of parameters (raster angle = 0°, layer thickness = 0.3 mm, infill density = 80%) illustrates the critical balance needed among the three influential factors to yield maximum performance.

Conclusion

This article evaluates the impact of raster angle, layer thickness, and infill density on the bending strength of specimens produced via fused filament fabrication (FFF). The experimental design and response surface methodology (RSM) were employed to validate the results. RSM facilitated the identification of optimal parameters and the analysis of both individual and interaction effects on bending strength with a minimal number of experiments. Statistical analysis indicated that a quadratic model best fits the experimental data. For the bending strength response in the bending test, the fourth specimen with density parameters of 80%, layer thickness of 0.3 mm, and raster angle of zero degrees has the best properties. The fifth specimen has the lowest properties, with parameters of infill density of 20%, layer thickness of 0.1 mm, and raster angle of 90 degrees. It has bending strength. The bending strength values for the fourth and fifth specimens are 54.18 and 9.8 MPa, respectively, and the average value equals 28.61 MPa. The influence of the density parameter on the bending properties shows that increasing the infill density improves the test response. By increasing the density of holes and gaps between layers, which are the points of stress concentration and the beginning of damage, it is reduced, and the properties are improved. Only this point should be kept in mind as the density of raw materials used increases, the cost and time of construction, and the weight of the piece also increase. In the mechanical properties of bending, the raster angle parameter was known to be the most influential parameter because it generally affects how the load is transferred inside the specimen. The raster angle of 0 degrees is the most suitable, and the angle of 90 degrees shows the lowest mechanical properties in experimental tests.

References

[1] M. Attaran, The rise of 3-D printing: The advantages of additive manufacturing over traditional manufacturing, Business Horizons, 60(5) (2017) 677-688.
[2] T.D. Ngo, A. Kashani, G. Imbalzano, K.T.Q. Nguyen, D. Hui, Additive manufacturing (3D printing): A review of materials, methods, applications and challenges, Composites Part B: Engineering, 143 (2018) 172-196.
[3] Y.L. Yap, W.Y. Yeong, Additive manufacture of fashion and jewellery products: a mini review, Virtual and Physical Prototyping, 9(3) (2014) 195-201.
[4] N. Mohan, P. Senthil, S. Vinodh, N. Jayanth, A review on composite materials and process parameters optimisation for the fused deposition modelling process, Virtual and Physical Prototyping, 12(1) (2017) 47-59.

[5] T.N.A.T. Rahim, A.M. Abdullah, H. Md Akil, Recent Developments in Fused Deposition Modeling-Based 3D Printing of Polymers and Their Composites, Polymer Reviews, 59(4) (2019) 589-624.
[6] V. Shanmugam, D.J.J. Rajendran, K. Babu, S. Rajendran, A. Veerasimman, U. Marimuthu, S. Singh, O. Das, R.E. Neisiany, M.S. Hedenqvist, F. Berto, S. Ramakrishna, The mechanical testing and performance analysis of polymer-fibre composites prepared through the additive manufacturing, Polymer Testing, 93 (2021) 106925.
[7] O.A. Mohamed, S.H. Masood, J.L. Bhowmik, Optimization of fused deposition modeling process parameters: a review of current research and future prospects, Advances in Manufacturing, 3(1) (2015) 42-53.
[8] A. Garg, A. Bhattacharya, An insight to the failure of FDM parts under tensile loading: finite element analysis and experimental study, International Journal of Mechanical Sciences, 120 (2017) 225-236.
[9] M. Dawoud, I. Taha, S.J. Ebeid, Mechanical behaviour of ABS: An experimental study using FDM and injection moulding techniques, Journal of Manufacturing Processes, 21 (2016) 39-45.
[10] J. Nomani, D. Wilson, M. Paulino, M.I. Mohammed, Effect of layer thickness and cross-section geometry on the tensile and compression properties of 3D printed ABS, Materials Today Communications, 22 (2020) 100626.
[11] A. Rodríguez-Panes, J. Claver, A.M. Camacho, The Influence of Manufacturing Parameters on the Mechanical Behaviour of PLA and ABS Pieces Manufactured by FDM: A Comparative Analysis, Materials, 11(8) (2018) 1333.
[12] S. Kannan, M. Ramamoorthy, Mechanical characterization and experimental modal analysis of 3D Printed ABS, PC and PC-ABS materials, Materials Research Express, 7(1) (2020) 015341.
[13] A. Khalili, A. Kami, V. Abedini, Tensile and Flexural Properties of 3D-Printed Polylactic Acid/Continuous Carbon Fiber Composite, Mechanics of Advanced Composite Structures, 10(2) (2023) 407-418.
[14] Y. An, L. Zhang, C. Chang, Z. Zhu, L. Xiong, C. Tang, X. Chen, G. Zhang, W. Gao, Research on the surface quality improvement of 3D-printed parts through laser surface treatment, Optics & Laser Technology, 181 (2025) 111711.
[15] P. Rendas, L. Figueiredo, M. Geraldo, C. Vidal, B.A. Soares, Improvement of tensile and flexural properties of 3D printed PEEK through the increase of interfacial adhesion, Journal of Manufacturing Processes, 93 (2023) 260-274.
[16] S. Zou, S. Cao, E. Yilmaz, Enhancing flexural property and mesoscopic mechanism of cementitious tailings backfill fabricated with 3D-printed polymers, Construction and Building Materials, 414 (2024) 135009.
[17] M.H. Esfe, S.N.H. Tamrabad, H. Hatami, S. Alidoust, D. Toghraie, Using the RSM to evaluate the rheological behavior of SiO2 (60%) - MWCNT (40%)/SAE40 oil hybrid nanofluid and investigating the effect of different parameters on the viscosity, Tribology International, 184 (2023) 108479.
[18] M. Hemmat Esfe, S. Alidoust, S.N. Hosseini Tamrabad, D. Toghraie, H. Hatami, Thermal conductivity of MWCNT-TiO2/Water-EG hybrid nanofluids: Calculating the price performance factor (PPF) using statistical and experimental methods (RSM), Case Studies in Thermal Engineering, 48 (2023) 103094.
[19] M.H. Esfe, S.M. Motallebi, H. Hatami, M.K. Amiri, S. Esfandeh, D. Toghraie, Optimization of density and coefficient of thermal expansion of MWCNT in thermal oil nanofluid and modeling using MLP and response surface methodology, Tribology International, 183 (2023) 108410.
[20] N. Vidakis, M. Petousis, A. Vairis, K. Savvakis, A. Maniadi, A parametric determination of bending and Charpy's impact strength of ABS and ABS-plus fused deposition modeling specimens, Progress in Additive Manufacturing, 4(3) (2019) 323-330.
[21] Z. Raheem, Standard Test Methods for Flexural Properties of Unreinforced and Reinforced Plastics and Electrical Insulating Materials 1, 2019.
[22] M. Samykano, S.K. Selvamani, K. Kadirgama, W.K. Ngui, G. Kanagaraj, K. Sudhakar, Mechanical property of FDM printed ABS: influence of printing parameters, The International Journal of Advanced Manufacturing Technology, 102(9) (2019) 2779-2796.

[23] S. Mahendran, S. Selvamani, K. Kadirgama, W. Ngui, K. Ganesan, Mechanical property of FDM printed ABS: influence of printing parameters, The International Journal of Advanced Manufacturing Technology, 102 (2019).
[24] T.Q. Tran, F.L. Ng, J.T.Y. Kai, S. Feih, M.L.S. Nai, Tensile Strength Enhancement of Fused Filament Fabrication Printed Parts: A Review of Process Improvement Approaches and Respective Impact, Additive Manufacturing, 54 (2022) 102724.